INTERNATIONAL JOURNAL OF PRECISION ENGINEERING AND MANUFACTURING Vol. 16, No. 11, pp. 2245-2254 OCTOBER 2015 / 2245
DOI: 10.1007/s12541-015-0289-5 ISSN 2234-7593 (Print) / ISSN 2005-4602 (Online)

Flexure-Hinges Guided Nano-Stage for Precision Manipulations: Design, Modeling and Control

Peng-Bo Liu[1], Peng Yan[1,2,#], Zhen Zhang[3,4], and Tong-Tong Leng[1]

1 Key Laboratory of High-efficiency and Clean Mechanical Manufacture, Ministry of Education, School of Mechanical Engineering, Shandong University, Jinan, Shandong, 250061, China
2 School of Automation Science and Electrical Engineering, Beihang University, Beijing, 100191, China
3 Department of Mechanical Engineering, Tsinghua University, Beijing, 100084, China
4 Beijing Key Lab of Precision/Ultra-Precision Manufacturing Equipment and Control, Tsinghua University, Beijing, 100084, China
Corresponding Author / E-mail: pengyan2007@gmail.com, TEL: +86-531-88392239, FAX: +86-531-88392239

KEYWORDS: Piezoelectric driven nano-stage, Hysteresis nonlinearity, Active Disturbance Rejection Control (ADRC), Extended State Observer (ESO)

In this paper, a novel piezoelectric actuator driven nano-stage with bridge type mechanism is studied from the perspectives of design optimization, dynamical modeling, as well as controller synthesis for high precision manipulation purposes. FEM (Finite Element Method) analysis and dynamical modeling are provided to derive the system model including the hysteresis nonlinearity. Considering the complexities of dynamical uncertainties and hysteresis nonlinearity, an active disturbance rejection controller is developed consisting of extended state observer (ESO), state feedback controller and profile generator. With the proposed algorithm, the nonlinear dynamics, system uncertainties and external disturbances can be treated as part of the "total disturbances", such that the extended state observer can be used to estimate and suppress the effects of these complex dynamics. The proposed control algorithm is deployed in real time implementations on the designed nano-stage, where experimental results demonstrate good control performance in terms of high precision positioning, hysteresis compensation and disturbance rejection.

Manuscript received: December 21, 2014 / Revised: May 9, 2015 / Accepted: July 21, 2015

1. Introduction

1.1 Background

High precision micro/nano-stage is a key component in many fields of precision engineering, such as high resolution imaging systems,[1] lithography machining of semiconductors,[2] as well as Hard Disk Drive (HDD) data storage systems.[3] Regardless of various application objectives and manipulating tasks, one of the common requirements for micro/nano-stages is the capability of positioning or moving with high resolution, high repeatability, and high bandwidth.[4] The design and control of micro/nano motion stages with ultra-high precision has become one of the key enabling technologies in these areas.

To satisfy the ultra-high precision requirements, most micro/nano stages are designed on the base of the compliant mechanism, which employ various flexure hinges to generate motions through elastic deformation.[5,6] The use of flexure hinges makes the nano-stages to eliminate the friction and clearance issues that exist in a traditional mechanism. The piezoelectric actuators have been widely used to drive the compliant mechanism due to their characteristics of large load capacity, high resolution and fast response. Accordingly, high resolution and high bandwidth sensors (e.g. laser displacement sensors or optical encoders) are incorporated in the nano-stage design, such that advanced feedback control algorithms can be deployed to achieve ultra-high precision manipulations. For compliant mechanism design, guiding mechanisms[7] and displacement amplification mechanisms[8] are necessary due to the coupling motion and the limited stroke of piezoelectric actuators. There are inevitable tradeoffs among the system stroke, bandwidth and working load in the mechanical structures design. Therefore the innovation and design optimization on nano-stages have attracted significant research, see e.g. Pucheta[9] and Shan[10] for references.

Although flexure hinges based nano-stage is a promising way to accomplish ultra-high precision manipulations, the natural hysteresis and creep nonlinearities limit the accuracy of the developed nano-stages. Moreover, various external disturbances will also reduce the positioning or moving precision of the system. In order to solve these problems, various research efforts have been made in the past few years. Charge control[11] is a successful method to suppress the hysteresis

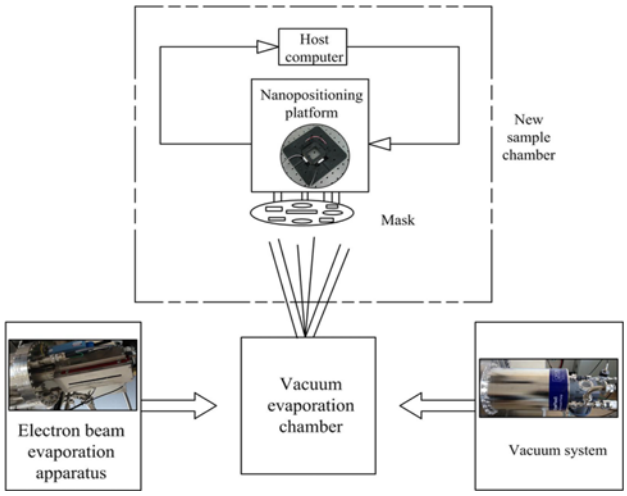

Fig. 1 Schematic plot of the direct writing vacuum evaporation system

effects. However, charge control reduces workspace and bandwidth of the piezoelectric actuators as well as increases complexity of the control hardware. Thus, voltage control is widely used for controlling nano-stages including feedforward control[12] and feedback control.[13] It should be noticed that the feedforward control are usually based on the inverse model. However, the accurate hysteresis dynamic models are usually complicated, and their inverse models are difficult to get practically, especially when robustness has to be addressed.[14] Although the feedback methods are more robust in suppression of the hysteresis nonlinearity,[15] model uncertainties together with the complex nonlinear behaviors, especially the hysteresis nonlinearity, make it difficult to establish the accurate dynamic model for the controller design and to obtain robust stability results.[16]

1.2 Motivation

The main purpose of this work is to investigate the analysis, design and control methods for nano-manipulating stages supporting a novel direct writing vacuum evaporation instrument for quantum device fabrications. As described in our previous work,[13] the system is composed of an electron beam evaporation apparatus, a vacuum system, a vacuum evaporation chamber, as well as a new sample chamber, as shown in Fig. 1. Based on the performance specifications of the equipment, strict requirements have been put forward for nano-stage design, such as bandwidth, stroke, resolution and vacuum compatibility. In the meanwhile the coating process inevitably results in various disturbances, such as vibration, environment temperature variation and sensor noise, which significantly affect the motion accuracy of the nano-stage. Considering the requirements on operating accuracy, geometry limitations, as well as anti-disturbance control performance, the nano-stage needs to be prototyped in a systematic way such that the mechanical design can be accurately achieved and its model can be analytically captured for anti-disturbance control purpose. It is worth noting that most existing results on the analysis of the amplification mechanisms are quite inconsistent with the practical performance in nano-stages. These deviations limit appropriate deployment of model based anti-disturbance control, such as disturbance-observer-based control,[17] internal model control,[18] etc.

With this, we consider the systematic design, modeling and control methods for a piezoelectric actuator driven nano-stage with a bridge type mechanism. In particular, we restrict our attention to the bridge-type amplifiers based design with a new analysis method facilitating more accurate design analysis, and the active disturbance rejection controller (ADRC)[19,20] approach is developed for the nano-stage to deal with the nonlinear dynamics, system uncertainties, as well as external disturbances.

1.3 Contribution

In the present paper, we aim to provide a systematic study on the design optimization, dynamical modeling, controller synthesis and experimental evaluations for a piezoelectric actuator driven nano-stage. In Particular, we focus on how to the accurately analyze and design the mechanical system and handle various model uncertainties and disturbances for ultra-high precise manipulation purpose.

One of the main contributions of this paper is a modified analysis method for bridge-type amplifiers. Comparing with existing analysis methods,[21,22] our new approach is more accurate to predict the performance of bridge-type mechanisms in nano-manipulating systems. Accordingly this method is applied to the mathematical modeling and optimizations of the bridge-type-amplifier based nano-stage, which is further verified by finite element analysis (FEA) results. Meanwhile, an active disturbance rejection control (ADRC) approach is proposed for nano-manipulations in the presence of various disturbances and model uncertainties. With the proposed algorithm, the nonlinear dynamics, system uncertainties and external disturbances are treated as part of the "total disturbances", and further estimated and actively compensated by the extended state observer (ESO). The proposed ADRC algorithm is deployed in real time implementations on the designed nano-stage, where experimental results demonstrate good control performance in terms of high precision positioning, hysteresis compensation and disturbance rejection.

The rest of the paper is organized as follows: A piezoelectric-actuator driven nano-stage is designed in Section 2, where the static model of the nano-stage is established for parameter optimization and further is verified by finite element analysis (FEA). In Section 3, a general model of the nano-stage is proposed and the system parameters are identified by experimental data. The active disturbance rejection controller (ADRC) based on extended state observer (ESO) is proposed to reject the "total disturbances" in Section 4. Experimental results for controlling the designed nano-stage in Section 5, followed by conclusions in Section 6.

2. Mechanical Design and Analysis

2.1 Mechanical design of the nano-stage

The schematic diagram of the designed piezoelectric-actuator driven nano-stage is depicted in Fig. 2. In the proposed nano-stage, the central motion platform is connected to the fixed frame through four leaf springs, which constitute a double four-bar parallelogram mechanism. Due to the leaf springs' characteristics of high longitudinal stiffness, low transverse stiffness and low stress concentration, the leaf parallelogram can well improve the nano-stage's rejection capability

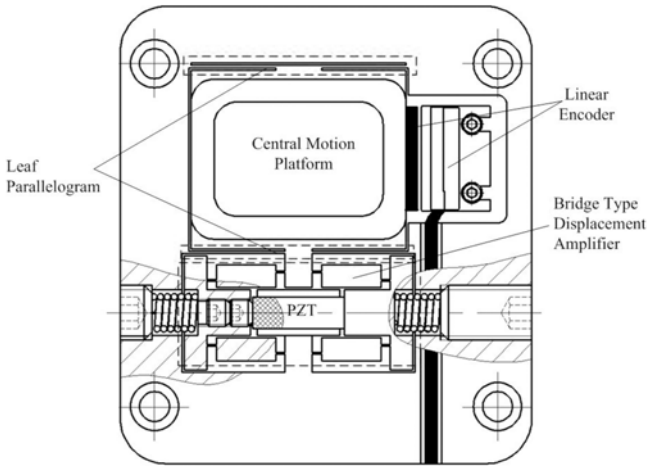

Fig. 2 Schematic diagram of the designed nano-stage

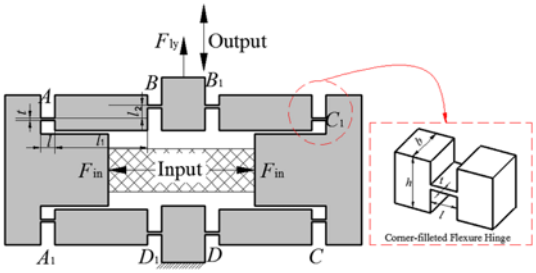

Fig. 3 A flexure-based bridge type displacement amplifier

against parasitic motions and other external disturbances. Therefore, the motion of the piezoelectric actuator can be transmitted to the central motion platform accurately.

A piezo stack is adopted as the actuator for the nano-stage, thanks to its characteristics of high resolution, high force, high stiffness and fast response. However, considering the fact that the stroke of the piezo stack is very limited and cannot meet the workspace requirement, a bridge type displacement amplification mechanism,[21,23] as shown in Fig. 3, which has a compact structure and a large displacement amplification ratio is employed in the developed nano-stage. Corner-filleted flexure hinges are used in this displacement amplifier because they are more flexible than other type flexure hinges of the same size.

2.2 Static modeling and parameters optimization

Various analytical models have been developed for bridge-type amplification mechanisms, based on the geometric relations,[24,25] elastic beam theory[21,22] and compliance matrix method.[26] However these methods cannot be directly applied to the static modeling of the nano-stage due to the effect of the reactive force from the guiding mechanism. Therefore, a new analysis method for bridge-type amplifiers is proposed in this section, where the static model of the nano-stage is also established for parameters optimization.

Thanks to the symmetrical structure of the bridge-type amplifier, only one bridge arm needs to be analyzed. Assume that each flexure hinge has a 3-DOF compliance which arises from the deformations, and the other elements are rigid bodies, as shown in Fig. 4. As illustrated

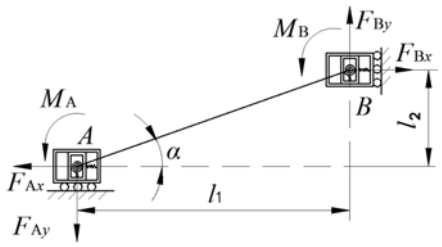

Fig. 4 Schematic of single arm of bridge-type amplifier

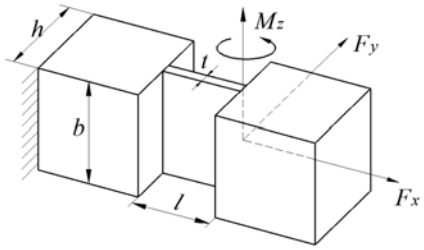

Fig. 5 Coordinate system of corner-filleted flexure hinges

in Fig. 5, the compliance equation of the flexure hinge can be written as follows:[21]

$$\begin{bmatrix}\delta x\\ \delta y\\ \delta\theta\end{bmatrix}=\begin{bmatrix}c_{11} & 0 & 0\\ 0 & c_{22} & c_{23}\\ 0 & c_{32} & c_{33}\end{bmatrix}\begin{bmatrix}\delta F_x\\ \delta F_y\\ \delta M_z\end{bmatrix}=\begin{bmatrix}\frac{l}{Ebt} & 0 & 0\\ 0 & \frac{4l^3}{2Ebt^3}+\frac{l}{Gbt} & \frac{6l^2}{Ebt^3}\\ 0 & \frac{6l^2}{Ebt^3} & \frac{12l}{Ebt^3}\end{bmatrix}\begin{bmatrix}\delta F_x\\ \delta F_y\\ \delta M_z\end{bmatrix}, \quad (1)$$

where $[\delta x, \delta y, \delta\theta]^T$ is the generalized displacement of the flexure hinge, $[\delta F_x, \delta F_y, \delta M_z]^T$ is the generalized force applied at the hinge, E is the material's Young's modulus, G is the shear modulus, and l, b, t represent the length, height and thickness of the corner-filleted flexure hinge respectively.

We denote F_{Ax}, F_{Ay} and F_{Bx}, F_{By} as the inverse forces imposed on hinge A and B respectively. Owing to the identical rotation angle of the two flexure hinges in arm AB, it is assumed that the internal moments caused by the two hinges are identical (i.e., M_A=M_B). Note that only the longitudinal reactive force F_{ly} is applied to the amplifier due to the symmetrical structure of the guiding mechanism, as shown in Fig. 3.

According to force and moment equilibrium, we have

$$F_{Ax}=F_{Bx}=F_x=\frac{F_{in}}{2}, \quad (2)$$

$$F_{Ay}=F_{By}=F_y=\frac{F_{ly}}{2}, \quad (3)$$

$$M_A=M_B=M=\frac{F_x l_2-F_y l_1}{2} \quad (4)$$

where F_{in} is the driving force imposed on the bridge-type mechanism, l_1 and l_2 represent the horizontal and vertical lengths of the rigid links respectively.

As shown in Fig. 4, the input and output displacements could be

divided into three parts: the deformations of flexure hinges A and B, and the rotation of rigid link AB. Flexure hinges A and B have the same elastic deformations due to the same force status. In addition, the rotation angle of the rigid link AB is identical to rotation angles of the flexure hinges (i.e., $\Delta\alpha = \delta\theta$). According to the Euler-Bernoulli beam theory and kinematic analysis, the following relationships can be derived:

$$\Delta x = 2\Delta x_l + l_2\Delta\alpha, \tag{5}$$

$$\Delta y = 2\Delta y_l + l_1\Delta\alpha, \tag{6}$$

where Δx and Δy represent the input and output displacements of the bridge arm respectively, Δx_l and Δy_l represent the translational deformations of the flexure hinges in x and y directions.

According to Eqs. (1)-(4), we can calculate the deformations of flexure hinges A and B. Then we have the input and output displacements of the bridge-type amplifier as

$$x_{in} = 2\Delta x = \frac{2l(t^2+3l_2^2)}{Ebt^3}F_{in} + \frac{6ll_2(l-l_1)}{Ebt^3}F_{ly}, \tag{7}$$

$$y_{out} = 2\Delta y = \frac{6ll_2(l+l_1)}{Ebt^3}F_{in} + \left(\frac{2l(2l^2-3l_1^2)}{Ebt^3} + \frac{2l}{Gbt}\right)F_{ly}. \tag{8}$$

For the guiding mechanism shown in Fig. 2, four leaf springs form the double four-bar parallelogram mechanism. Due to the symmetrical structure and identical working conditions, only one leaf spring is analyzed to establish the mathematical model. The mechanics analysis of one leaf spring PQ is illustrated in Fig. 6. According to the bending deformation theory,[27] we can have the deflection equation for leaf spring as

$$w(x) = \frac{F_{sq}x^2(3l_s-2x)}{Eb_st_s^3}, \tag{9}$$

where b_s, t_s and l_s represent the height, thickness and initial length of the leaf spring PQ respectively, F_{sq} is the shear force imposed on the endpoint Q.

Note that the driving force F_s imposed on the guiding mechanism and the force F_{ly} imposed on the amplifier are an action-reaction pair, which can be derived as

$$F_s = F_{ly} = 4F_{sq} = \frac{4Eb_st_s^3}{l_s^3}y_{out}. \tag{10}$$

As the whole nano-stage is manufactured monolithically, the height of the bridge-type amplifier is identical to the guiding mechanism (i.e., $b_s = b$). Substituting Eq. (10) into Eqs. (7) and (8), we can have

$$x_{in} = \frac{2\gamma ll_s^3(t^2+3l_2^2)+144\lambda^3l^2l_2^2(l^2-l_1^2)}{\gamma Ebt^3l_s^3}F_{in}, \tag{11}$$

$$y_{out} = \frac{6ll_2(l+l_1)}{\gamma Ebt^3}F_{in}. \tag{12}$$

where

$$\lambda = \frac{t_s}{t}, \quad \gamma = 1 - \frac{8\lambda^3l(2l^2-3l_1^2)+16\lambda^3lt^2(1+\mu)}{l_s^3},$$

and μ is the Poisson's ratio of the material.

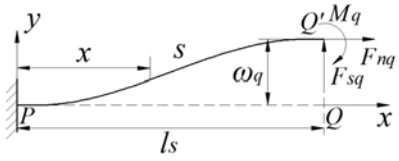

Fig. 6 Mechanics analysis of one leaf spring

Table 1 Critical parameters of the nanostage

Structure Parameters (mm)						
t	b	l	l_1	l_2	l_s	t_s
0.4	15	2	13	1.4	15	0.8
Material Parameters						
Young's modulus		Yield strength		Poisson's ratio		Density
71.9 GPa		455 MPa		0.33		2810 Kg/m^3

Then we can obtain the displacement amplification ratio of the nano-stage as

$$R_{amp} = \frac{6ll_2(l+l_1)l_s^3}{2l(t^2+3l_2^2)(l_s^3-16\lambda^3lt^2(1+\mu))+16\lambda^3l^2(3l^2l_2^2+3l_1^2t^2-2l^2t^2)}. \tag{13}$$

In addition, the input stiffness K_{in} and the equivalent stiffness K_{eq} of the nano-stage can be derived as

$$K_{in} = \frac{\gamma Ebt^3l_s^3}{2\gamma ll_s^3(t^2+3l_2^2)+144\lambda^3l^2l_2^2(l^2-l_1^2)}, \tag{14}$$

$$K_{eq} = \frac{\gamma Ebt^3}{6ll_2(l+l_1)}. \tag{15}$$

The fundamental natural frequency can be calculated by

$$f = \frac{1}{2\pi}\sqrt{\frac{K_{eq}}{M}}, \tag{16}$$

where M is the equivalent mass of the nano-stage.

In this design, the proposed nano-stage is expected to satisfy the following objectives: 1) the workspace of the nano-stage is around 100 μm; 2) the natural frequency should be over 300 Hz. To this end, the material of nano-stage is chosen as aluminum alloy AL7075-T6 with high ratio of yield strength to Young's modulus. It is noticeable that the performance of the nano-stage is highly dependent on some dimensional parameters. Recall Eqs. (11)-(16) with additional considerations on the constraints of allowable stress, size limitation, and the features of the piezo actuators. The dimensional parameters of the nano-stage are optimized as shown in Table 1. As a result, the proposed nano-stage achieves a displacement amplification ratio of 4.8 and a high natural frequency of 412.46 Hz.

2.3 Design validation with FEA

The designed nano-stage is verified by Finite-Element Method (FEM). The static and modal analysis is carried out by FEA method to verify the design. The static analysis results are illustrated in Fig. 7. It is clear that the developed nano-stage has an amplification ratio of 4.7 according to the FEA results, which is fairly consistent with the theoretical value, as shown in Table 2. The tiny displacement loss is mainly due to the reason that the links of the compliant mechanisms are

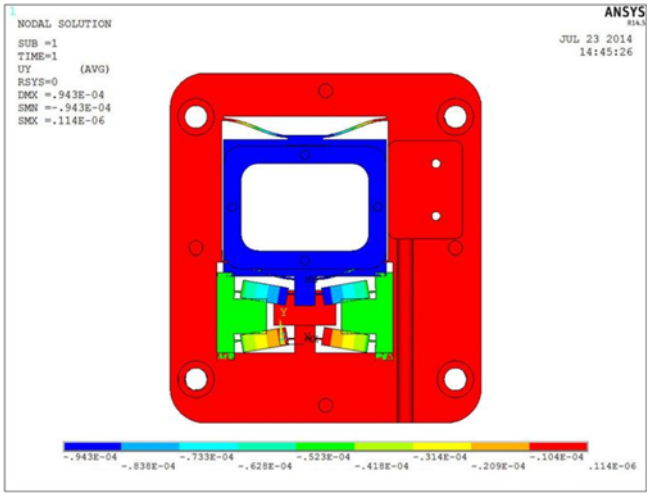

Fig. 7 Static analysis results of the nano-stage

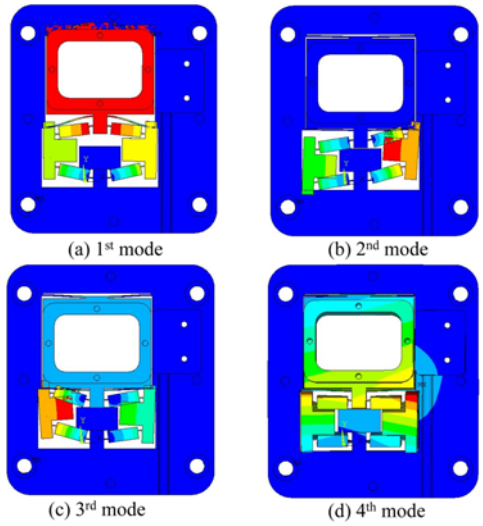

Fig. 8 First four modes of the nano-stage obtained by ANSYS

Table 2 Analysis results of the nano-stage

Method	Our method	Method in Ref[21]	Method in Ref[22]	FEA
Amplification ratio	4.8	8.3	8.2	4.7

Table 3 ANSYS results on frequency modes

Modes	1st	2nd	3rd	4th
Frequency (Hz)	421.77	821.77	904.87	1778.94

not rigid bodies, thus generate deformations under stress. Meanwhile it can be clearly shown that the existing models for bridge-type amplifiers have considerable errors to predict the performance of the bridge-type amplifier based nano-stages, as shown in Table 2. Besides, the first four mode shapes extracted by ANSYS are shown in Fig. 8 and the corresponding frequencies are listed in Table 3. It is obvious that the theoretical calculation of the natural frequency agrees well with the FEA results.

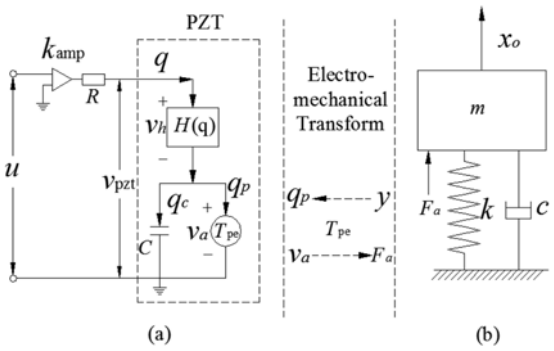

Fig. 9 The electromechanical model of piezoelectric driven nano-stage: (a) electrical part and (b) mechanical part

3. Dynamical Modeling and Identification

3.1 Electromechanical coupling modeling

The dynamic model of the piezoelectric actuator driven nano-stage can be represented by Fig. 9, which consists of the electrical part (Fig. 9(a)) and the mechanical part (Fig. 9(b)). The electric modeling is composed of a circuit of the voltage amplifier and an equivalent circuit of piezoelectric actuator (PZT). Practically the voltage amplifier is simplified as a fixed gain k_{amp} with an equivalent resistance R. Considering the hysteresis effect, the piezoelectric effect and the capacitive characteristic of the PZT, the PZT is modeled as a serial connection of a nonlinear hysteresis unit $H(q)$ and a parallel structure of an electromechanical transducer with transformer ratio T_{pe} and an equivalent capacitance C. Then we define the total charge in PZT is q, and the resulting current flowing through the circuit is $\dot{q}$. As shown in Fig. 9(b), the mechanical part can be simplified as a mass-spring-damper system.

Based on the Kirchhoff law, Newton's law and the piezoelectric effect, the following dynamical of the piezoelectric driven nano-stage can be obtained as

$$\dddot{y}+a_2\ddot{y}+a_1\dot{y}+a_0y=b_0u-b_1H(q) \tag{17}$$

where

$$a_2=c/m+1/C,\quad a_1=(kC+T_{pe}^2+c)/mC,$$
$$a_0=(kRC+RT_{pe}^2-T_{pe}^2)/mRC^2,$$
$$b_0=T_{pe}k_{amp}/mRC,\quad b_1=T_{pe}/mRC,$$

$y(t)$ is the output displacement of the nano-stage, m, k, c are the equivalent mass, stiffness and damping coefficient of the nano-stage, respectively.

3.2 System parameters identification

Recall the system model (17), the linear portion of the dynamics is a third-order linear system, without considering the nonlinear hysteresis effect $H(q)$. According to the experimental frequency response data, the nominal system dynamics can be identified as:

$$G(s)=\frac{\overline{b}_0}{s^3+\overline{a}_2s^2+\overline{a}_1s+\overline{a}_0}=\frac{5.125\times10^5}{s^3+5810s^2+1.085\times10^7s+3.524\times10^{10}} \tag{18}$$

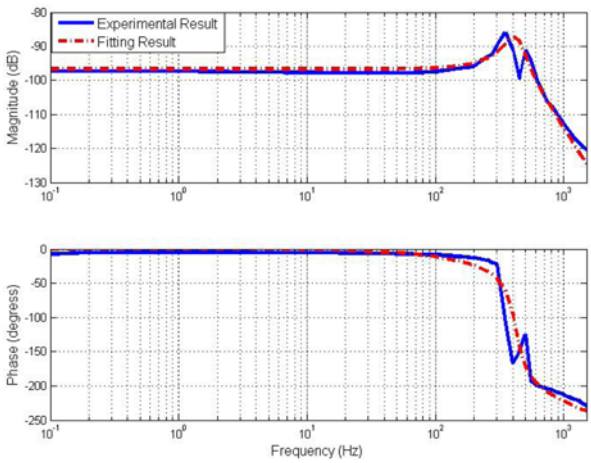

Fig. 10 Open-loop frequency responses

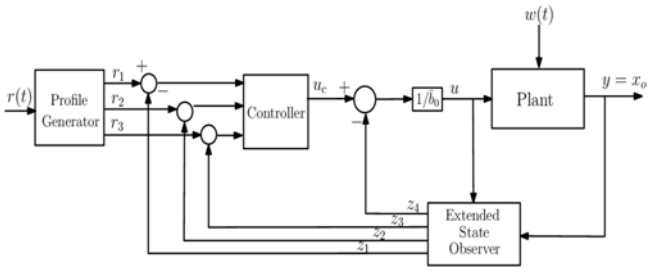

Fig. 11 Block diagram of active disturbance rejection control

Fig. 10 shows the comparison between the frequency responses of the experimental data (blue solid line) and identification results (red dash-dot line). It clearly demonstrates that the third-order model with the estimated parameters in Eq. (18) can reasonably capture the system's dynamics. Note that the system resonance peak appears at around 360 Hz, which is a bit lower than the natural frequency of 421.77 Hz derived from FEA in Section 2. The discrepancy is mainly due to the machining error which reduces the stiffness of the flexure hinges.

4. Active Disturbance Rejection Control

Note that the flexible modes are inevitable in the control of the nano-stages, which pose major challenge for nano-manipulations. As described in last section, nonlinear hysteresis effect always exits and complicates the control task due to the multivalued and nonlocal memoryless property. In addition, various disturbances seriously affect the manipulating accuracy. Therefore, in order to deal these challenges, we propose an active disturbance rejection control method (as shown in Fig. 11) for the nano-stage. Under the effect of the extended state observer (ESO), ADRC use an approximated simple dynamical model for the system design, instead of an accurate model of the plant, which is complexly nonlinear because of the hysteresis nonlinearity. Besides, this method also doesn't require accurate information of external disturbances.

Considering the existence of external disturbance $\omega(t)$, the plant model Eq. (17) can be rewritten as

$$\begin{aligned}\dddot{y} &= -a_2\ddot{y}-a_1\dot{y}-a_0y+\bar{b}_0u+(b_0-\bar{b}_0)u-b_1H(q)+\omega \\ &= \bar{b}_0u+f(\ddot{y},\dot{y},y,u,\omega,H(q),t)\end{aligned} \tag{19}$$

where $f(\cdot)$ is defined as the "total disturbances" including both the internal dynamics $-a_2\ddot{y}-a_1\dot{y}-a_0y+\bar{b}_0u+(b_0-\bar{b}_0)u-b_1H(q)$ and the external disturbance $\omega(t)$.

Since the "total disturbances" is unknown, an extended state observer is designed to estimate and compensate it, which treat $f(\cdot)$ as an additional state of system Eq. (19). We assume that $f(\cdot)$ is differentiable and define the state variables as $x(t) = [x_1, x_2, x_3, x_4]^T = [y, \dot{y}, \ddot{y}, f]^T$. Then the plant model Eq. (19) can be transformed into the following state space form

$$\begin{aligned}\dot{x} &= Ax+Bu+E\dot{f} \\ y &= Cx\end{aligned} \tag{20}$$

where

$$A=\begin{bmatrix}0&1&0&0\\0&0&1&0\\0&0&0&1\\0&0&0&0\end{bmatrix},\ B=\begin{bmatrix}0\\0\\\bar{b}_0\\0\end{bmatrix},\ E=\begin{bmatrix}0\\0\\0\\1\end{bmatrix},\ C=\begin{bmatrix}1&0&0&0\end{bmatrix}.$$

Referring to reference,[28] we have the extended state observer (ESO) as

$$\begin{aligned}\dot{z} &= Az+Bu+L(y-\hat{y}), \\ \hat{y} &= Cz,\end{aligned} \tag{21}$$

where $z = [z_1, z_2, z_3, z_4]^T$ represents the observer state which provides an estimation of the system state x, and $L = [L_1, L_2, L_3, L_4]^T$ is the observer gain is chosen such that all the observer poles are at $-\omega_o$. That is

$$L = [4\omega_o \quad 6\omega_o^2 \quad 4\omega_o^3 \quad \omega_o^4]^T. \tag{22}$$

With a well-tuned ESO, the "total disturbances" f will be estimated by the observer state z_4, that is $z_4 \approx f$. As depicted in Fig. 11, the control law is designed as

$$u = \frac{u_c-z_4}{\bar{b}_0}. \tag{23}$$

Substituting control law Eq. (23) into plant model Eq. (19), we have the augmented system as

$$\dddot{y} = u_c-z_4+f \approx u_c, \tag{24}$$

which means that the "total disturbances" f is actively compensated by ESO. Therefore, the original plant Eq. (19) is reduced to a unit gain triple integrator Eq. (24) which can easily controlled using the following state feedback controller

$$u_c = k_1(r_1-z_1)+k_2(r_2-z_2)+k_3(r_3-z_3), \tag{25}$$

where $r_1 = \dot{r}$, $r_2 = \ddot{r}$, $r_3 = \dddot{r}$, r is the reference signal, and the state feedback controller gain $K = [k_1, k_2, k_3]$ is chosen as $K = [\omega_c^3, 3\omega_c^2, 3\omega_c]$, placing all the closed-loop poles at $-\omega_c$.

It should be noted that the above parameters are selected based on following considerations:[29]

1) The controller bandwidth should be higher than the bandwidth of closed feedback system that we desired;

2) The observer bandwidth should be three to five times higher than

Table 4 Values of the controller and observer gains

ω_c	450 Hz
ω_o	1800 Hz
k_1	2.26×10^{10}
k_2	2.39×10^{7}
k_3	8.48×10^{3}
L_1	4.52×10^{4}
L_2	7.67×10^{8}
L_3	5.78×10^{12}
L_4	1.63×10^{16}

the controller bandwidth;

3) The observer bandwidth should be five to ten times less than the sampling frequency.

Considering high-speed and high-precision motion requirements, we select the state feedback controller bandwidth ω_c as 450 Hz, and the observer bandwidth ω_o as fourth times higher than the controller bandwidth. Then the observer and controller gains L and K can be determined respectively, as listed in Table 4.

5. Implementation and Experimental Results

5.1 Experimental setup

Based on the design and analysis results presented in Section 2, a prototype of the proposed nano-stage was monolithically machined by AL 7075-T6 using the wire electrical discharge machining (WEDM) technique thanks to its accuracy and precision. An experimental apparatus for control and implementation purposes is then established as depicted in Fig. 12, where the piezoelectric-actuator driven nano-stage is mounted to a floatation platform for the vibration suppression purpose. Considering the high bandwidth and high precision requirements of the piezoelectric actuator, a very high bandwidth voltage amplifier is designed to drive the piezo stack. A *RENISHAW* laser interferometer is installed for real time displacement measurement. Besides, we employ Matlab/Simulink real time control package xPCTarget with National Instruments (*NI*) PCI-6251 I/O hardware for feedback control implementations.

5.2 Implementation and experimental results

The developed control algorithm is further implemented on the experimental apparatus depicted in Fig 12. A sampling frequency of 10 kHz is chosen to avoid possible aliasing effects during the experiments and ensure high bandwidth control implementations. The frequency responses of the closed-loop system are illustrated in Fig. 13. The results demonstrate that the bandwidth of the closed-loop systems is around 100 Hz. Particularly, the sensitivity plots indicate good disturbance rejection capability of the proposed ADRC, as shown in Fig. 13(a).

Fig. 14 shows the step response of the closed-loop control system which only uses the designed active disturbance rejection controller. The settling time for the output response is about 14 ms and the overshoot is eliminated. Furthermore, the steady-state error indicates that the positional accuracy is less than 10 nm. The above results demonstrate that the nano-stage has good performance in the high-speed and high-precision positioning control by applying the proposed

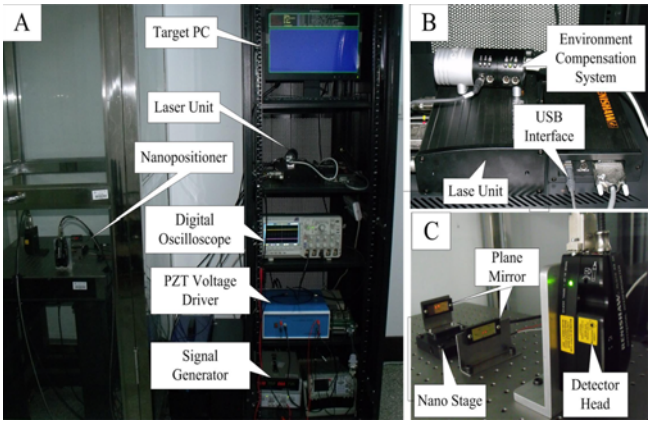

Fig. 12 (A) Experimental setup (B) Details of laser interferometer (C) Prototype of the piezoelectric-actuator driven nano-stage

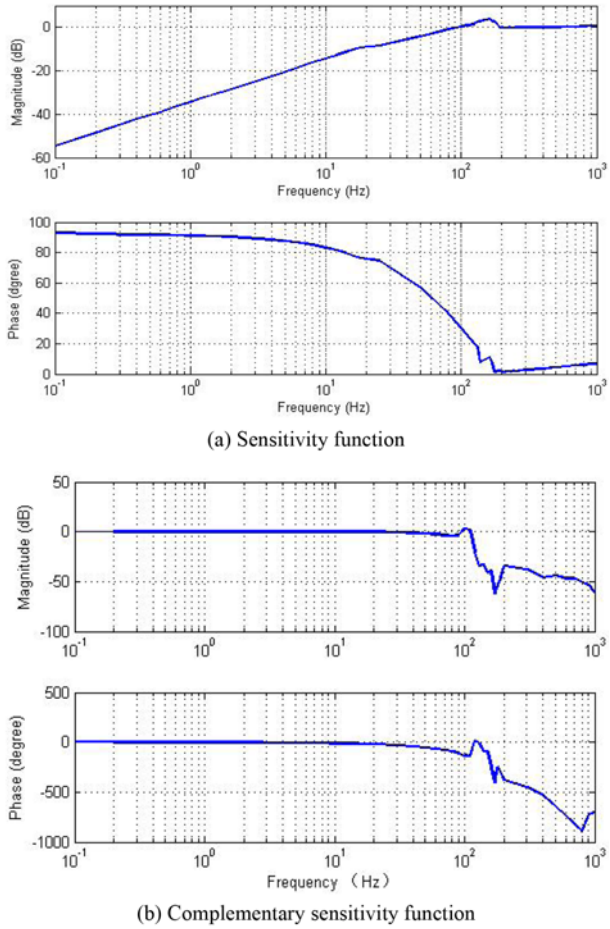

Fig. 13 Closed-loop frequency responses

active disturbance rejection controller.

Moreover, Fig. 15 shows the experimental results of the active disturbance rejection controller to track a sinusoidal signal of $r(t) = 25\sin(10\pi t + \pi/2)+25$ (μm). It demonstrates that the tracking error is less than 0.53 μm. The RMS tracking error can be calculated as 0.33 μm, which demonstrates that an average tracking error less than 1.1% can be obtained by the active disturbance rejection controller.

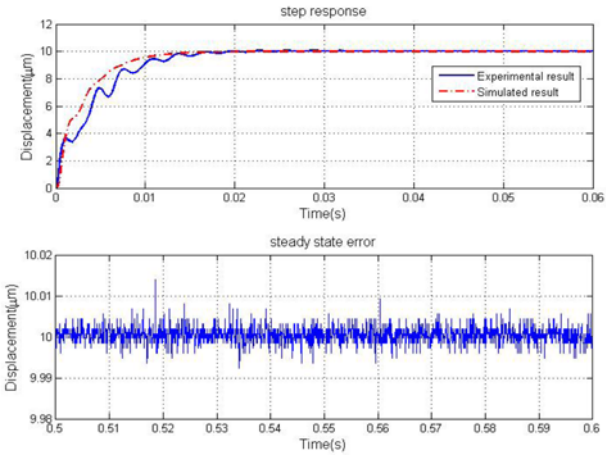

Fig. 14 Experimental results of step response

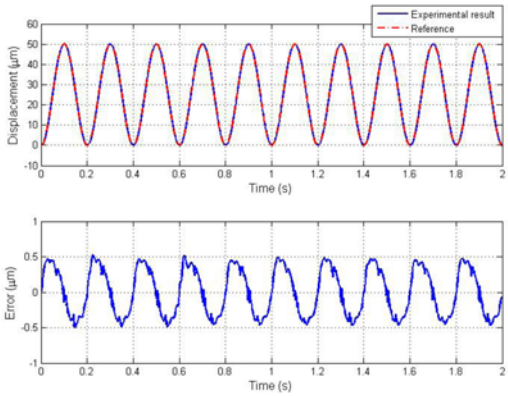

Fig. 15 Experimental results of tracking performance

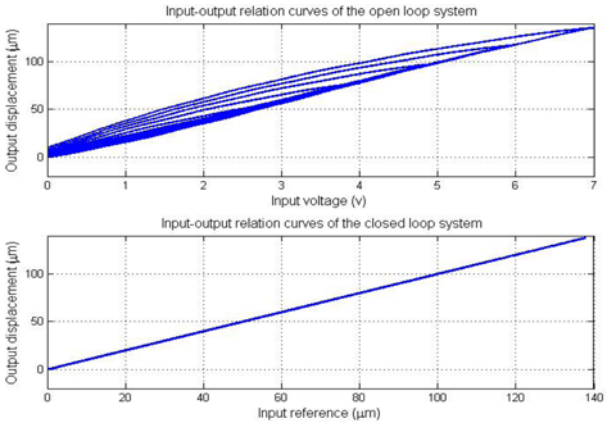

Fig. 16 Experimental results of the hysteresis compensation

Apart from the excellent tracking performance, the developed control structure of ADRC also demonstrates good hysteresis compensation ability, as shown in Fig. 16. The experimental results show that the maximum gap of the open-loop hysteresis curve is around 22 μm, which is reduced to less than 60 nm with the effect of the controller. The hysteresis nonlinearity is well eliminated and the relationship between the input and output of the system is approximately linear.

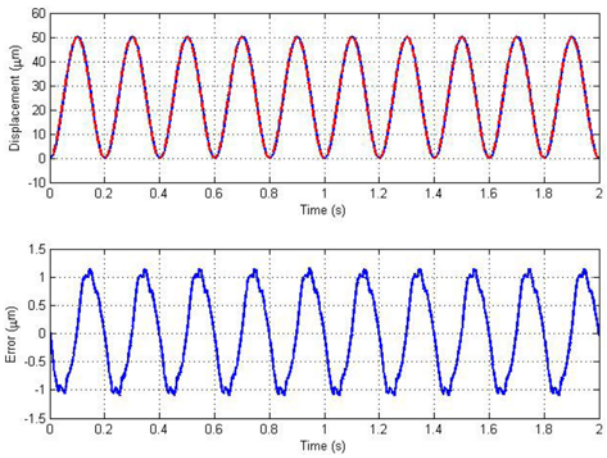

Fig. 17 Tracking performance of PID controller

To further verify the performance of the proposed controller, comparative experiments are also deployed between the designed ADRC and the conventional PID controller. Fig. 17 depicts the experimental results of the PID controller to track the same sinusoidal signal. The maximum tracking error of PID controller is 1.15 μm, while our ADRC controller achieves maximum tracking error of 0.53 μm, which demonstrates 53.9% performance improvement in tracking.

6. Conclusions

In this paper, we proposed a comprehensive study on the design, modeling, controller synthesis and experiment evaluations for a bridge-type-amplifier based nano-stage. We developed a new analysis method for bridge-type amplifiers, which is more accurate than existing methods. Accordingly, the static model of the nano-stage was established for parameters optimizations, and then verified by FEA. The dynamical model of the nano-stage was obtained by electromechanical analysis and experimental data identification. For the purpose of nano-manipulations, an active disturbance rejection controller (ADRC) was designed for an approximated third order model, which can effectively estimate and compensate the "total disturbances" including nonlinear dynamics, system uncertainties and external disturbances. Real time control implementations demonstrated that the proposed control algorithm achieved excellent positioning and tracking performance with good anti-disturbance capabilities. Current work along this line of research includes disturbance observer based control and internal-model based high precision tracking for nano-manipulation purposes.

ACKNOWLEDGEMENT

We would like to thank the financial support from the NSFC (grant No. 61327003 and 61004004), China Fundamental Research Funds for the Central Universities under Grant No. 10062013YWF13-ZY-68 and 10062014YWF-14-ZDHXY-018, Tsinghua University Initiative Scientific Research Program (grant no. 2010Z02270) and Specialized

Research Fund for the Doctoral Program of Higher Education (grant no. 20100002120043).

REFERENCES

1. Tien, S., Zou, Q., and Devasia, S., "Iterative Control of Dynamics-Coupling-Caused Errors in Piezoscanners during High-Speed AFM Operation," IEEE Transactions on Control Systems Technology, Vol. 13, No. 6, pp. 921-931, 2005.
2. Shinno, H., Yoshioka, H., and Taniguchi, K., "A Newly Developed Linear Motor-Driven Aerostatic X-Y Planar Motion Table System for Nano-Machining," CIRP Annals-Manufacturing Technology, Vol. 56, No. 1, pp. 369-372, 2007.
3. Abramovitch, D. and Franklin, G., "A Brief History of Disk Drive Control," IEEE Control Systems, Vol. 22, No. 3, pp. 28-42, 2002.
4. Gu, G.-Y., Zhu, L.-M., Su, C.-Y., and Ding, H., "Motion Control of Piezoelectric Positioning Stages: Modeling, Controller Design, and Experimental Evaluation," IEEE/ASME Transactions on Mechatronics, Vol. 18, No. 5, pp. 1459-1471, 2013.
5. Liu, P., Yan, P., and Zhang, Z., "Design and Analysis of an X-Y Parallel Nanopositioner Supporting Large-Stroke Servomechanism," Proceedings of the Institution of Mechanical Engineers, Part C: Journal of Mechanical Engineering Science, Vol. 229, No. 2, pp. 364-376, 2014.
6. Yong, Y. K., Moheimani, S. O. R., Kenton, B. J., and Leang, K., "Invited Review Article: High-Speed Flexure-Guided Nanopositioning: Mechanical Design and Control Issues," Review of Scientific Instruments, Vol. 83, No. 12, Paper No. 121101, 2012.
7. Li, Y., Xiao, S., Xi, L., and Wu, Z., "Design, Modeling, Control and Experiment for a 2-DOF Compliant Micro-Motion Stage," Int. J. Precis. Eng. Manuf., Vol. 15, No. 4, pp. 735-744, 2014.
8. Jung, H. J. and Kim, J. H., "Novel Piezo Driven Motion Amplified Stage," Int. J. Precis. Eng. Manuf., Vol. 15, No. 10, pp. 2141-2147, 2014.
9. Pucheta, M. A. and Cardona, A., "Design of Bistable Compliant Mechanisms using Precision-Position and Rigid-Body Replacement Methods," Mechanism and Machine Theory, Vol. 45, No. 2, pp. 304-326, 2010.
10. Shan, Y. and Leang, K. K., "Design and Control for High-Speed Nanopositioning: Serial-Kinematic Nanopositioners and Repetitive Control for Nanofabrication," IEEE Control Systems, Vol. 33, No. 6, pp. 86-105, 2013.
11. Chen, L.-S., Yen, J.-Y., Chen, J. J. H, Kuo, F.-C, Chen, M.-S., Chen, Y.-Y., and Chung, B.-I., "Precision Tracking of a Piezo-Driven Stage by Charge Feedback Control," Precision Engineering, Vol. 37, No. 4, pp. 793-804, 2013.
12. Nguyen, P.-B. and Choi, S.-B., "Micro-Position Control of a Piezostack Actuator using Rate-Dependent Hysteretic Compensator," Int. J. Precis. Eng. Manuf., Vol. 12, No. 5, pp. 885-891, 2011.
13. Liu, P., Yan, P., Zhang, Z., and Leng, T., "Modeling and Control of a Novel X-Y Parallel Piezoelectric-Actuator Driven Nanopositioner," ISA Transactions, Vol. 56, pp. 145-154, 2015.
14. Clayton, G. M., Tien, S., Leang, K. K., Zou, Q., and Devasia, S., "A Review of feedforward Control Approaches in Nanopositioning for High-Speed SPM," Journal of Dynamic Systems, Measurement, and Control, Vol. 131, No. 6, Paper No. 061101, 2009.
15. Devasia, S., Eleftheriou, E., and Moheimani, S. R., "A Survey of Control Issues in Nanopositioning," IEEE Transactions on Control Systems Technology, Vol. 15, No. 5, pp. 802-823, 2007.
16. Gu, G.-Y., Zhu, L.-M., Su, C.-Y., Ding, H., and Fatikow, S., "Modeling and Control of Piezo-Actuated Nanopositioning Stages: A Survey," IEEE Transactions on Automation Science and Engineering, DOI No. 10.1109/TASE.2014.2352364, 2014.
17. Kim, W., Shin, D., Won, D., and Chung, C. C., "Disturbance-Observer-based Position Tracking Controller in the Presence of Biased Sinusoidal Disturbance for Electrohydraulic Actuators," IEEE Transactions on Control Systems Technology, Vol. 21, No. 6, pp. 2290-2298, 2013.
18. Sun, Z., Zhang, Z., and Tsao, T.-C., "Trajectory Tracking and Disturbance Rejection for Linear Time-Varying Systems: Input/Output Representation," Systems & Control Letters, Vol. 58, No. 6, pp. 452-460, 2009.
19. Gao, Z., "Scaling and Bandwidth-Parameterization based Controller Tuning," Proc. of the American Control Conference, pp. 4989-4996, 2006.
20. Zhao, S. and Gao, Z., "An Active Disturbance Rejection based Approach to Vibration Suppression in Two-Inertia Systems," Asian Journal of Control, Vol. 15, No. 2, pp. 350-362, 2013.
21. Ma, H.-W., Yao, S.-M., Wang, L.-Q., and Zhong, Z., "Analysis of the Displacement Amplification Ratio of Bridge-Type Flexure Hinge," Sensors and Actuators A: Physical, Vol. 132, No. 2, pp. 730-736, 2006.
22. Qi, K.-Q., Xiang, Y., Fang, C., Zhang, Y., and Yu, C.-S., "Analysis of the Displacement Amplification Ratio of Bridge-Type Mechanism," Mechanism and Machine Theory, Vol. 87, pp. 45-56, 2015.
23. Xu, Q. and Li, Y., "Analytical Modeling, Optimization and Testing of a Compound Bridge-Type Compliant Displacement Amplifier," Mechanism and Machine Theory, Vol. 46, No. 2, pp. 183-200, 2011.
24. Pokines, B. J. and Garcia, E., "A Smart Material Microamplification Mechanism Fabricated using LIGA," Smart Materials and Structures, Vol. 7, No. 1, pp. 105, 1998.
25. Lobontiu, N. and Garcia, E., "Analytical Model of Displacement Amplification and Stiffness Optimization for a Class of Flexure-based Compliant Mechanisms," Computers & Structures, Vol. 81, No. 32, pp. 2797-2810, 2003.
26. Kim, J. H., Kim, S. H., and Kwak, Y. K., "Development and

Optimization of 3-D Bridge-Type Hinge Mechanisms," Sensors and Actuators A: Physical, Vol. 116, No. 3, pp. 530-538, 2004.

27. Yuanqiang, L. and Wangyu, L., "Analysis of the Displacement of Distributed Compliant Parallel-Guiding Mechanism Considering Parasitic Rotation and Deflection on the Guiding Plate," Mechanism and Machine Theory, Vol. 80, pp. 151-165, 2014.
28. Zheng, Q., Gao, L. Q., and Gao, Z., "On Validation of Extended State Observer through Analysis and Experimentation," Journal of Dynamic Systems, Measurement, and Control, Vol. 134, No. 2, Paper No. 024505, 2012.
29. Zhao, S. and Gao, Z., "Modified Active Disturbance Rejection Control for Time-Delay Systems," ISA transactions, Vol. 53, No. 4, pp. 882-888, 2014.